DEM study of the porosity distribution of pellet sandpile formed by ternary size particles

Wei, Han; Ge, Yao; Li, Meng; Li, Ying; Saxén, Henrik; He, Zhijun; Yu, Yaowei

Published in:
Powder Technology

DOI:
10.1016/j.powtec.2019.11.017

Published: 15/01/2020

Document Version
Accepted author manuscript

Document License
CC BY-NC-ND

DEM study of the porosity distribution of pellet sandpile formed by ternary size particles

Han Wei[1], Yao Ge[1], Meng Li[1], Ying Li[1], Henrik Saxén[2], Zhijun He[3] and Yaowei Yu[1*]

1. State Key Laboratory of Advanced Special Steel, Shanghai Key Laboratory of Advanced Ferrometallurgy, School of Materials Science and Engineering, Shanghai University, China
2. Thermal and Flow Engineering Laboratory, Department of Chemical Engineering, Åbo Akademi University, Biskopsgatan 8, FI-20500 Åbo, Finland
3. School of Material and Metallurgical Engineering, University of Science and Technology LiaoNing, China

*Corresponding author: E-mail: yaoweiyu@shu.edu.cn

Abstract

Porosity is an important parameter to reflect the internal structure of the heap, and it is related to the permeability of a packed bed. Thus, understanding and further adjusting the porosity distribution will help to control the gas-solid reaction in a chemical reactor. In this work, sandpiles formed by ternary size particles with variable mass ratio were researched by discrete element method. The porosity increases with the increase of the mass fraction of small particles. Different dump methods (Drop Test and Chute Test) both cause four distinct porosity regions (Zone A, B, C and D), but the locations are not the same. Changing the drop height in Drop Test and chute properties in Chute Test both have influence on the porosity zone, especially for the upper porosity. Furthermore, size segregation will lead to uneven porosity distribution, but there is no evident relationship between porosity and size segregation in sandpile.

Key words: Discrete element method, porosity distribution, pellet sandpile, ternary size particles

1 Introduction

Sandpile formed by various dump methods of granular matter is common in many areas. It has long been a hot topic for many theorists and practitioners due to the ever-increasing requirement of understanding the properties of bulk sandpile [1-3]. The main contents of these studies include repose angle [1, 4],packing fraction [5-9], stress distribution [4, 10], porosity [11-13] and particle segregation of a sandpile. Sandpile is the main body of a packed bed. Packed bed reactors in the chemical industry and engineering have prompted extensive studies [14]. In particular, porosity of packed bed is a significant properties in gas-solid processes encountered in chemical reaction engineering [15, 16].

Microscopic study of packed bed includes porosity, void fraction and packing density of the bed with single size spheres [2, 17, 18], multi-size spheres [19, 20] and non-spherical mixtures [21]. In blast furnace (BF) ironmaking, porosity of lump zone have great effect on gas distribution and chemical reactions between raw materials (bulk particles) and the gas. Besides porosity, size segregation is also used to reflect the bed structure and is widely used in the studies of blast furnace, which is easier to do qualitative or quantitative research in experiments and simulations. Therefore, many researchers [22-26] try to study the phenomenon, reasons and impacts of size segregation happened in the charging and discharging process of BF [27-29], liquid fluidized beds [30-33] and rotating drum [34] by experimental and simulated methods. In particular, the mass fraction of different particle sizes has obvious effects on size segregation. Only a few studies have focused on particle size segregation in the conical piles, which is a basis of packed bed. Some of them are aimed at binary particle system. Thomas [35] studied the mixtures of two types of glass beads in a funnel to form a pile. They found that for large size difference, there is a segregation of the large beads at the surface of the flowing phase, but with small size difference, the large beads segregate inside. Rahman et al. [36] analyzed the size segregation mechanism of binary particle mixture in forming a conical pile and found the zone, where the segregating component

of smaller particle is contained around a central feed point. As for ternary system, Hong et al. [37] studied the segregation of glass beads in three-sectional tapered fluidized beds and revealed that the separation efficiency of glass beads increased with increasing initial mass fraction of small particles. However, there are fewer papers studying both the porosity and size segregation in the packed bed. In fact, porosity is an important factor directly reflecting permeability in classical Ergun equation and is a constant. Even a small change of voidage along vertical direction of the bed would significantly influence the permeability, gas distribution, chemical reaction and temperature distribution of the whole bed. Li et al. [38] have studied the relationship of voidage distribution and segregation in green bed formed on iron ore sinter strand, which demonstrated that the voidage and vertical size segregation have positive correlation. Therefore, in the process of ironmaking, the horizontal and whole porosity distribution or segregation are also important and worth studying.

The research on porosity of packed bed can be divided into direct physical measurements and numerically method, including mathematical calculation [21, 39, 40], numerical simulation [11, 41] and so on. Honestly, there are some difficulties for the experimental research of the porosity distribution as the opacity of a pile and discontinuity and randomness of particles in it. Therefore, some new technologies, such as X-ray radiography [42], X-ray computed tomography [43], gamma ray computed tomography [44] and magnetic resonance imaging [45] have been employed. Recently, Khalili et al. [43] using X-ray computed tomography to explore the porosity-depth variation below a porous media interface of multi-sized spherical or arbitrarily-shaped granules. However, these methods are mainly aimed at small-scale experiments and smaller particles. For large-scale experiments, even factory scale, it will be very difficult. In addition, experimental studies often require considerable work force, financial resources and time. Therefore, some researchers tend to mathematical calculation [21, 39, 40]. Most of the studies focused on the distribution of porosity in containers. A.Yu [20] developed a packing model from the viewpoint of the microstructure of particles to predict porosity of packed bed and also studied the

packing porosity of binary particle system[46]. Mueller [47] proposed that using geometrical and analytical techniques and arc lengths to calculate the radial porosity profile of mono-sized spheres in packed bed cylinders. Recently, He [48] gave a scaling approach method for the independent radial variable, which was applied to an existing empirical correlation model. In fact, it's relatively easy for the measurement of the porosity of packed bed in a container either in experiment or in simulation. Because of the difficulty in porosity measurement and expression, until now, there are still few public reports about 3D porosity distribution of a sandpile formed by natural pilling and the effects of mass fraction of particle sizes on porosity distribution of sandpile. Nikola et al. [2] studied the distribution of packing fraction in a very large 3D heap of monodisperse spherical particles and revealed that the packing fraction of single-particle sandpile can be divided into four distinct packing fraction (density) regions. He [2] used the Visscher-Bolsterli (VB) algorithm, which provides a realistic framework for rapid computation and allows investigating very large assemblies of particles. Numerical analysis is often an attractive option, which can be used to directly study the porosity of a packed bed. For example, the gas flow distribution and non-uniform heat loss in packed beds are numerically investigated by predicting the porosity distribution through Monte Carlo Simulation [49]. An accurate prediction of local porosity (a constant value) by Ergun Equation is also used for stability heat transfer analysis of a packed bed [50, 51]. Discrete element method (DEM) [52], which can consider the information of every particle and the internal structure of the bulk, has become a vigorous tool for research on the behavior of granular matter.

This paper will address two different dump methods on porosity distribution of pellet piles and the effects of mass ratio of ternary size pellets on porosity distribution of a conical pile. We will first study the physical parameters (coefficient of rolling and static friction between particles) of pellet through measuring repose angles of heaps by DEM method and experimental verification. Then we will study the effects of the dump methods and mass ratio of ternary particles on porosity distribution and explore the relationship of the porosity and size segregation of the heap. In addition, we will pay

much attention to the mechanism of the change of porosity distribution in a conical heap.

2 Experimental work

Experimental work is used to determine the DEM parameters and to ensure the accuracy of the follow-up numerical simulation. There are various ways such as injection, discharging, and tilting methods [4, 53, 54] to form a sandpile. In order to reduce effect of surroundings on sandpile and easy to measure the porosity distribution in experiment, this work is performed by the second method (discharging). The experimental study is based on iron oxide pellets. As the shape of the pellet is close to that of a sphere, spherical particles were used in the simulations to be presented. In fact, particle shape affects the porosity of the pile, but since we focused on the pellets, particle shape was not considered. Pellets used in experiments came from a steel plant in China and about 10,000 pellets were selected after applying sieves with aperture size in the range of 13-15 mm. The experimental apparatus is illustrated in **Fig. 1**, which is a 1:10 scale charging system of an actual BF. A stable pellet pile was formed on a table by the discharging method. In order to study the profiles of the arising pile, a camera with the lens level along the desktop, was used to take photographs from four different directions of the pile. The angle of repose was obtained by analyzing the profile of the heap using photograph-processing technology.

The same method was used to form a pile for measuring the porosity distribution. Seven breakers (plexiglass) of 25 mL placed beforehand to be buried in the pellet pile were slowly removed afterwards to measure the porosity (P). We used drainage method to measure the porosity. Firstly, we poured the water from a measurement cylinder into a beaker with full of pellets. When the beaker is full of the water, we marked the volume change of the water in the measurement cylinder. The water volume can be used to represent the void among pellets. The measurement is very quick, and less than five seconds. Therefore, the adsorption of the pellets can be ignored. The porosity can be calculated by

$$P = \frac{V_0}{V} \tag{1}$$

where V_0 is the volume (mL) of pores, V is the volume of the empty beaker (mL), and P is the porosity. The experiments were repeated nine times and average values of each three groups of measurements were analyzed.

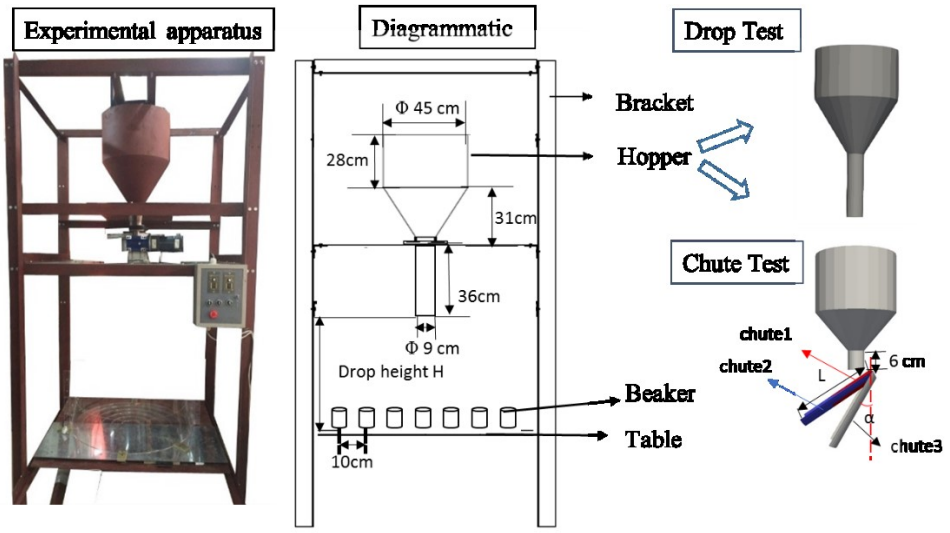

Fig. 1 Experimental apparatus (left) and diagrammatic (medium) of the measurement of pellet sandpile by Drop Test and Chute Test (right) (H: the distance from exit of the hopper to the table, α: angle between vertical line and central bottom line of chute, L: the length of the chute)

3 Simulation details

3.1 Discrete element method (DEM)

The simulation part of this research is based on DEM ,which was firstly proposed by Cundall and Strack [52] in 1979. This method considers two types of motion of a particle, translation and rotation, which are governed by Newton's second low of motion. The elastic contact force expression used in this work is the non-linear Hertz-Mindlin no-slip model [55], which is illustrated in **Fig. 2**. The basic expressions are given in Eqs. (2) and (3). The former is the translational equation, which is composed of gravitational force, m_ig, contact force and viscous contact damping force, where K_n, K_t , γ_n and γ_t express the normal elastic constant, tangential elastic constant, normal

damping constant and tangential damping constant, respectively. A particle with the mass of m_i contacts with K particles, and the contact force between them depends on the deformation (δ_n) between particles. In the equation, u_i, v_n and v_t represent the translational velocity, and the component of relatively velocity for the normal and tangential directions.

$$m_i \frac{du_i}{dt} = \sum_{j=1}^{K}\left(\mathrm{K_n}\delta n_{ij} - \gamma_\mathrm{n} v n_{ij}\right) + \left(\mathrm{K_t}\delta n_{ij} - \gamma_\mathrm{t} v t_{ij}\right) + m_i \mathrm{g} \tag{2}$$

Equation (3) represents the rotational movement of particles, where $\boldsymbol{M}_r^k$ and $\boldsymbol{M}_r^d$ are two torques caused by a tangential force and rolling friction, respectively. A Coulomb-type friction law is used to express the friction between two particles. I_i and ω_i denote the moment of inertia and rotational velocity, respectively.

$$I_i \frac{\mathrm{d}\omega_i}{\mathrm{d}t} = \sum_{j=1}^{K}(M_r^k + M_r^d) \tag{3}$$

Table 1 presents the formulas used to calculate the forces and torques between the particles. In this work, we use the open-source software LIGGGHTS 3.5.0 [56, 57] to implement DEM.

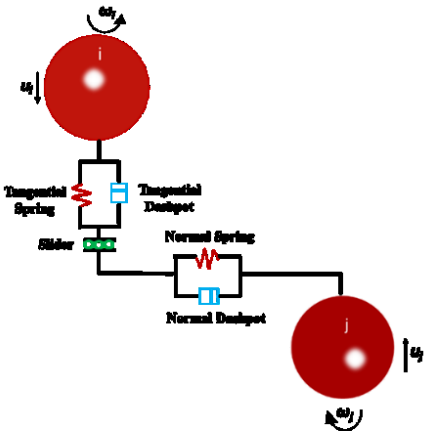

Fig. 2 Depiction of interaction forces between two particles (i and j) in DEM.

Table 1 Components of interaction forces and torques between particles

Coefficients	Equations
Elastic constant for normal and tangential K_n, K_t	$K_n = \frac{4}{3}\gamma^*\sqrt{R^*\delta_n}$, $K_t = 8G^*\sqrt{R^*\delta_n}$
Elastic damping constant for normal and tangential contact γ_n, γ_t	$\gamma_n = -2\sqrt{\frac{5}{6}}\beta\sqrt{s_n m^*} \gg 0$, $\gamma_t = -2\sqrt{\frac{5}{6}}\beta\sqrt{s_t m^*} \gg 0$

Sn, St	$S_n = 2\gamma^*\sqrt{R^*\delta_n}$, $S_t = 8G^*\sqrt{R^*\delta_n}$
β	$\beta = \frac{\ln(e)}{\sqrt{ln^2(e)+\pi^2}}$
$\frac{1}{\gamma^*}$	$\frac{1}{\gamma^*} = \frac{(1-v_i{}^2)}{Y_i} + \frac{(1-v_j{}^2)}{Y_j}$
$\frac{1}{G^*}$	$\frac{1}{G^*} = \frac{2(2-v_i)(1+v_i)}{Y_i} + \frac{2(2-v_j)(1+v_j)}{Y_j}$
$\frac{1}{R^*}$, $\frac{1}{m^*}$	$\frac{1}{R^*} = \frac{1}{R_i} + \frac{1}{R_j}$, $\frac{1}{m^*} = \frac{1}{m_i} + \frac{1}{m_j}$
ΔM_r^k	$\Delta M_r^k = -k_r \Delta\theta_r$, $k_r = k_t \cdot R^{*2}$
	$\lvert M_{r,t+\Delta t}^k \rvert \ll M_r^m$
	$M_{r,t+\Delta t}^k = M_{r,t}^k + \Delta M_r^k$, $M_r^m = \mu_r R^* F_n$
$M_{r,t+\Delta t}^d$	$M_{r,t+\Delta t}^d = -C_r\dot{\theta}_r(\lvert M_{r,t+\Delta t}^k \rvert < M_r^m)$
	$M_{r,t+\Delta t}^d = -C_r\dot{\theta}_r(\lvert M_{r,t+\Delta t}^k \rvert = M_r^m)$
	$C_r = \eta_r C_r^{crit}$, $C_r^{crit} = 2\sqrt{I_r k_r}$
	$I_r = (\frac{1}{I_i + m_i r_i^2} + \frac{1}{I_j + m_j r_j^2})^{-1}$

In the table, R_i and R_j are the radius of particles, m_i and m_j are the mass of particle i and j. F_t and F_n are the tangential and normal force, respectively. *Y, G, υ* and *e* define the Young's modulus, Shear modulus, Poisson's ratio and the coefficient of restitution, respectively. k_t, C_r, μ_r and μ_s express the tangential hardness, the damping coefficient, the coefficient of rolling and static friction, respectively.

3.2 Simulation contents

Simulations in the paper are divided into two parts. The first part is about the repose angle and BPD (bottom porosity distribution) of the heap formed by single size particles (14mm), which is used to calibrate physical parameters of pellets. The simulations were carried out by Drop Test (cf. middle Figure in **Fig. 1**), which is the same as the discharging method in experiment. The number of particles is 1×10^4 in this part to be consistent with the experiment. **Table 2** shows the DEM parameters. In particular, the coefficient of inter-particle static friction and rolling friction were determined by comparing the experimental and simulated repose angle of pellet piles. The geometric model consists of a hopper, a baffle and a table (cf. **Fig. 1**), which are the same as that used in the experiment. We also used actual boxes to measure the porosity distribution in the part of verification of physical parameters. Seven boxes with the size of 5 x 5 x

5 cm on the central line of the bottom of the sandpile are used to obtain BPD of pellet pile. In each box, the total volume of particles is calculated by the number of particles in the region multiplied by the volume of a single particle. It is worth noting that a particle is taken to belong to the box if its center coordinate are in the box for ease of calculation. The porosity of each box can be calculated by Eq. (4).

$$P = \left(1 - \frac{nV_p}{V}\right) \times 100\% \tag{4}$$

Where n is the numbers of particles, V_p is the volume of a single particle, V is the volume of the box.

In the second part, we used two methods to form the pellet pile, which are the Drop Test and Chute Test and the size of the geometry models are shown in **Fig. 1**. For the drop Test, more detail about the experiment process can be found in the previous work [13]. For the Chute Test, particles slide down on the chute after leaving the hopper, and then fall to the table to form a sandpile. In this part, we used virtual units (without box) to acquire the porosity in different positions of the pile to avoid the so-called "wall effect". For the convenience, the pile can be divided into multi-layers and each layer can be sub-divided into small units with same size to study the porosity distribution. **Fig. 3** shows the schematic diagram of different layers (X-axis) of porosity distribution, which are along the vertical direction (Z-axis), including layer1, layer2, layer3 and so on (from bottom to top), and along the Y-axis, including layer1, F1, F2, and so on. In this part, we will study the effects of mass ratio of ternary size particles on porosity distribution of different layers in the piles formed by two methods. The number of simulated particles is 1×10^5, which consist of small particles (S, 8mm in size), medium particles (M, 14mm) and large particles (L, 20mm). In addition, the external conditions may influence the porosity distribution of the sandpile. For Drop Test, we will study the effects of drop height on porosity distribution. For Chute Test, we will observe the effects of chute properties (length, inclined angle) on porosity distribution.

Table 2 Physical and contact parameters in DEM simulation

Parameters	Values
Particle number	100000
Particle density	4837 kg/m^3
Time step	10^{-5}s
Young's modulus	2.5×10^{10}Pa(pellet), 2×10^{10}Pa(steel plane), 7.2×10^{10}(plexiglass)
Poisson ratio (p-p; p-w; p-g)	0.25, 0.3, 0.2
Coefficient of restitution (p-p; p-w; p-g)	0.4, 0.35, 0.2
Coefficient of friction (p-w; p-g)	0.4, 0.25
Coefficient of rolling friction (p-w; p-g)	0.4, 0.15
Size of pellet	8mm, 14mm, 20mm

In the table, p-p, p-w and p-g represent the coefficients for pellet-pellet, pellet-wall and pellet-plexiglass (breaker) interaction.

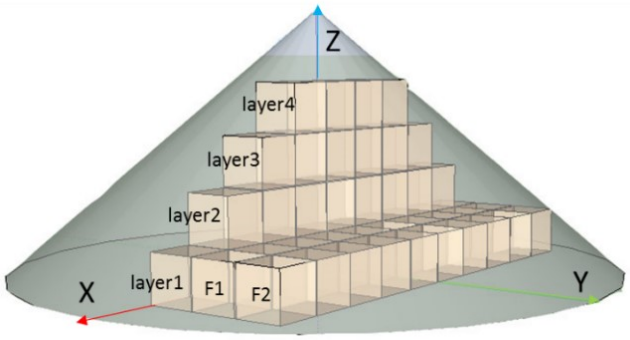

Fig. 3 Schematic diagram of different layers of porosity distribution. Layer 1, 2, 3and 4 represent the layers along the vertical center of the pile (Z-axis), F1 and F2 (F3…) represent the layers along the horizontal of the pile

4 Results and discussions

4.1 Verification of DEM physical parameters

The accuracy of physical parameters is very important to the authenticity of simulation research. We mainly studied the influence of the coefficient of static and rolling friction on repose angle of pellet sandpile. When studying the effects of one parameter on repose angle, other physical parameters are kept unchanged at the values reported in **Table 2**. **Table 3** is the deviation of repose angles between experiment and simulation with

different coefficients of rolling (μ_r) and static friction (μ_s). When the coefficient of rolling friction is 0.12 and coefficient of static friction is 0.15, the deviation (d) of repose angle between experiment and simulation is evidently the minimum. **Fig. 4** shows that the simulated free surface of the heap is consistent with experimental one.

In order further to verify the validity of the selected physical parameters, we used simulated and experimental methods to study the BPD of the piles formed by single size particles**.** Pellet piles and the beakers full of pellets, which are used to measure the bottom porosity distribution are shown in **Fig. 5**. **Fig. 6** shows the comparison of experimental and simulated porosity distribution when the coefficient of rolling friction is 0.12 and coefficient of static friction is 0.15 in simulation. Coordinate 0.00 of X-axis represents the center position of the pile and ±0.15m represents the edge. The trend of curves are almost the same in experiments and calculations. Thus, these two parameters can be used for further research.

Table 3 Deviation of repose angle between experiment and simulation with different coefficient of rolling and static friction

	Group	**Coefficient of friction**	**Equal value of four directions of heap(°) θ_e**	**Deviation from Experiment (%) d**
μ_s (when μ_r=0.1)	1	0.01	12.9	55.7
	2	0.15	24.5	15.9
	3	0.3	31.2	7.1
μ_r(when μ_s=0.15)	4	0.01	20.6	29.3
	5	0.12	27.9	4.1
	6	0.4	32.2	10.7
Experiment(θ)	-	-	29.1	-

In the table, μ_r and μ_s are the coefficients of rolling and static friction. d is the deviation of the repose angle of simulation from experiment, which can be calculated by $d = \frac{|\theta_e - \theta|}{\theta} \times 100\%$. θ_e and θ are the equal value of repose angle of four directions for different coefficient of rolling (static) friction and the experiment, respectively.

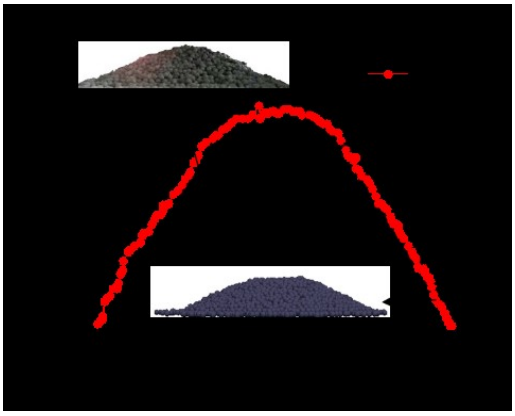

Fig. 4 Comparisons of the free surface of the pellet sandpile in simulation (Drop Test) and experiment (discharging method).

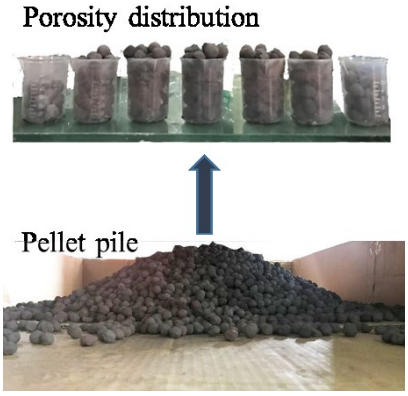

Fig. 5 Experimental photos of pellet piles and the beakers full of pellets, which are used to measure the bottom porosity distribution

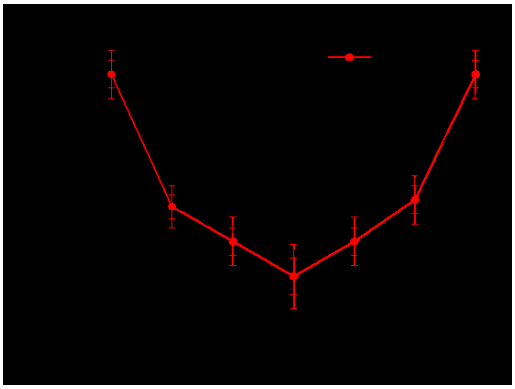

Fig. 6 Comparisons of the simulated and experimental BPD of the pellet sandpile formed by single size particles

4.2 Study on porosity distribution

4.2.1 Effects of mass ratio on porosity distribution

Mass ratio of different particle sizes as well as the dump methods of sandpile are all significant aspects for porosity distribution of a heap. We have designed different cases for these studies, which are all shown in **Table 4**. Mass ratio 1 and 2 in **Table 4** represent two changes of mass fraction of three particle sizes in simulations. For Mass ratio 1, mass fraction of small and medium particles both decreases at a rate of 10% but large particles increases at a rate of 20%. For Mass ratio 2, the mass fraction of medium particles remains unchanged, only large and small particle change. **Fig. 7** is the curves of porosity distribution of layer 1(cf. **Fig. 3**) of the sandpile formed by different mass ratios and dump methods. **Fig. 7** (a), (b), (c) and (d), (e), (f) show the relationship of porosity and size segregation of the sandpile. We used mass fraction of small particles to represent the segregation. **Fig. 7**(a) and (b) show that there is generally an increasing trend of the porosity with the increase of the mass ratio of small particles to large particles. Comparing **Fig. 7** (a) and (b), it can be seen that there is little effects of mass fraction of medium particle on the radial porosity distribution. Therefore, the porosity mainly depends on the mass fraction of small and large particles. In the Drop Test, porosity distribution of layer1 shows a symmetrical structure and the change of porosity distribution along the X-axis is not obvious, but the porosity at the center (x=0) is smaller than the edge(x=±0.5). **Fig. 7**(c) shows that the effect of mass ratio of three sizes on porosity of Chute Test is weaken than that of the Drop Test. A reason may be that the chute plays a role in particle redistribution and reduces the impact of different mass ratios.

Table 4 Cases of the mass ratio of different particle sizes and formation methods of sandpile

Mass ratio	Formation method	**Cases**	**Mass ratio of particles of different size (wt. %)** Small particles(S)	Medium particles(M)	Large particles(L)
Mass ratio 1	Drop test	Case A1	20	10	70
		Case A2	30	20	50
		Case A3	40	30	30

		Case A4	50	40	10
Mass ratio 2	Drop test and Chute test	Case B1	20	20	60
		Case B2(A2)	30	20	50
		Case B3	40	20	40
		Case B4	50	20	30

In **Fig. 7** (d), (e) and (f), the mass fractions of small particles at the center of the heap of different mass ratios are very close to each other, especial for Drop Test 1. Therefore, it's obvious that larger raw mass fraction of small particles will cause segregation fluctuates along the X-axis. The middle position is the main aggregation region of small particles to cause a large mass fraction of small particles. For convenience, **Fig. 8** is 2D cross-sections through the center of the heap, which are used to intuitively express the packing of particles in the heap. By observing the falling process of the particles in **Fig. 8** (1), we found that the particles falling from the top would flow separately because of different particle sizes. Large particles will fall vertically and deposit under the exit, but the small and medium particles will flow to both sides of the pile due to the percolation or even the rebound. However, in the Chute Test, porosity distribution in the right half of the piles (close to the chute) is larger than that in the left half, thus forming an asymmetric structure. The reasons can be seen from **Fig. 8** (2). Size segregation of particle occurs when pellet move on the chute as a result that small particles will fill the voids caused by large particles and deposit close to the chute bottom. In addition, when particles flow out of the chute, large particles in the upper of the chute will preferentially fall on the left slope of the pile but small particles (blue color) will fall on the right slope. Therefore, size segregation will lead to uneven porosity distribution. However, there is no obvious relationship between porosity and size segregation comparing (a), (b), (c) and (d), (e), (f). High porosity doesn't mean high segregation along the radial direction of the sandpile because porosity is a complex result of particle matching of different particle sizes. Thus, it is meaningful to study the change of porosity of the bed to control permeability and further control gas-solid reaction.

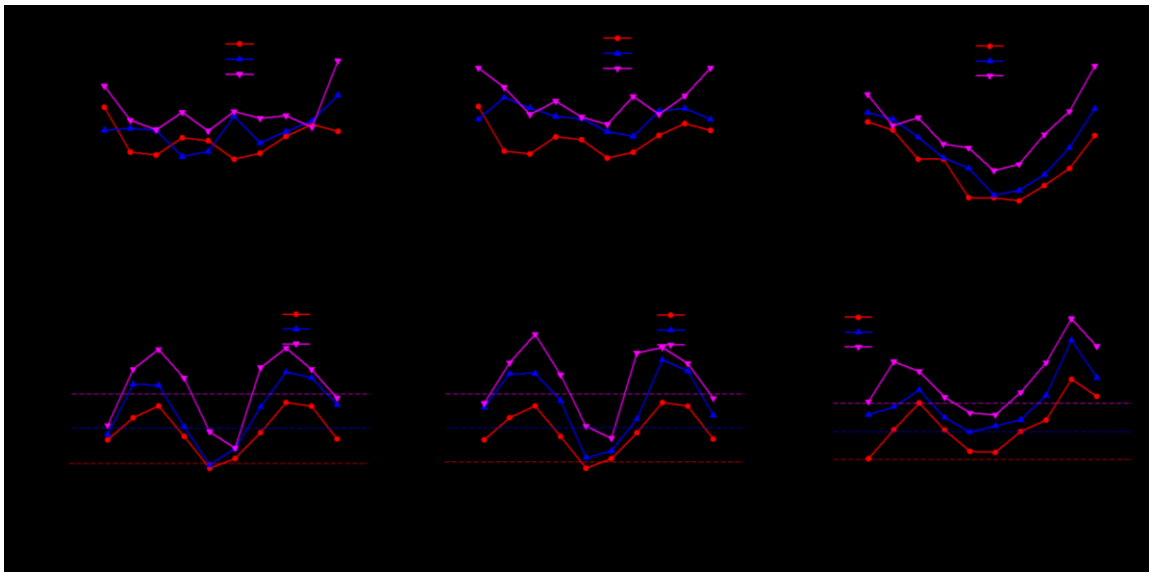

Fig. 7 The porosity distribution (upper figures) and the corresponding mass fraction of small particles (lower figures) of layer1 (X-axis) with different original mass ratio (S/M/L) and dump method. The dotted lines in the lower pictures represent the original mass fraction of small particles of this case.

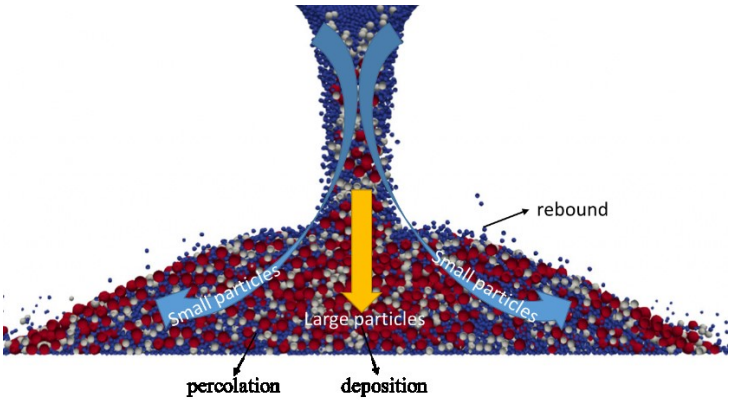

(1)

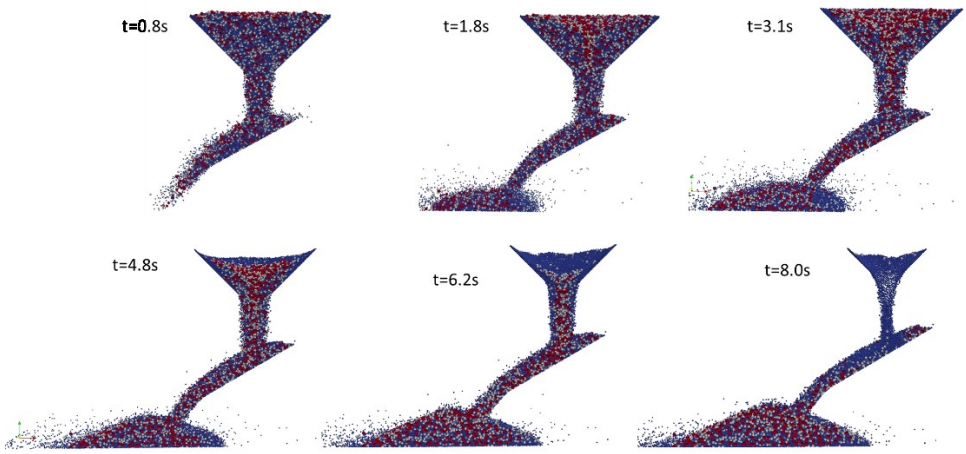

(2)

Fig. 8 2D screenshots of the discharging process of simulated Drop Test (1) and different state of the Chute Test (2) when the mass ratio (S: M: L) is 3:2:5 and the chute is chute1 (L=0.6m, α=60°). Different colors represent different particle size: blue, gray and red represent small, medium and large particles, respectively.

To further understand the porosity distribution in the sandpile, we have drawn a schematic (cf. **Fig. 9**) to express the regions with different particle sizes according to the calculated porosity of the heap in **Fig. 9**, which show the vertical cross-slice through the center of real heap formed by two methods. Nikola et al. [2] used Visscher-Bolsterli (VB) algorithm to calculate packing density of a heap, which is deposited by a large number of single-size particles, and found that heaps contain four distinct density (packing) region. In general, we also found that heaps formed by ternary size particles include four distinct porosity regions: Zone A, Zone B, Zone C and Zone D (cf. **Fig. 9**). The average porosity is Zone A<B<C<D. In both dump methods, Zone A is a particle-mixing region dominated by small particles. The reasons may be that the percolation phenomenon of small particles in the hopper so that some of them gathered at the exit of the hopper before opening, when the exit opened, they would fall out and form the layer on the table firstly. There is obvious a percolation phenomenon of small particles after they falling onto the table and forming a pile. Small particles are filled into the voids of large particles and are arranged regularly near the wall to cause a dense structure. Therefore, Zone A has minimum porosity. The above observation is consistent with those of previous experimental [58] and DEM work [25]. Zone B begin

to form after the stabilization of Zone A. In the Drop Test, large particles will "run" vertically out of the exit by gravity and are not prone to roll or rebound on the surface of the pile but just deposit. In the Chute Test, there will be percolation segregation on the chute. Large particles in the upper layer of chute firstly fall to the table and form Zone B, where is away from the chute. When B grows, parts of the small particles and medium particles will form Zone C. Final outflow of small particles will form a pure small particle area, Zone D, due to the segregation in the process of the hopper discharging [25]. Because the hopper is funnel flow type and the size segregation of pellet on the hopper makes small particles move to the void among large ones near the wall. Therefore, large particles tend to move to the zone in the center of the funnel flow during discharging process and the small particles flow out finally. Different dump methods will influence the location of Zone D, which depends on the hopper exit.

After the division of the different regions, we can easily find that the porosity distribution of the sandpile varies greatly along the vertical direction (porosity at the central position of different layers) in **Fig. 10,** which is formed by different mass ratios and dump methods. Porosity increases rapidly at first and then the speed is slowing down with the increase of the height of the sandpile. From the second layer to the top of the pile, the porosity increases, which can be explained from **Fig. 9**. The mass fraction of small particles increases gradually because of the finally flow of the small particles out of the funnel. Comparing (a) and (b) in **Fig. 10**, we found that the increase of porosity ($Z>-0.3$) in vertical direction in mass ratio 2 is more obvious than that in mass ratio 1. The difference between the two tests is whether the mass fraction of medium particles has changed, thereby increasing the mass fraction of small and medium particles (mass ratio 1) will reduce the change of porosity in the vertical direction. A reason may be that the medium particles will also occupy the voids between large particles to prevent the percolation of small particles.

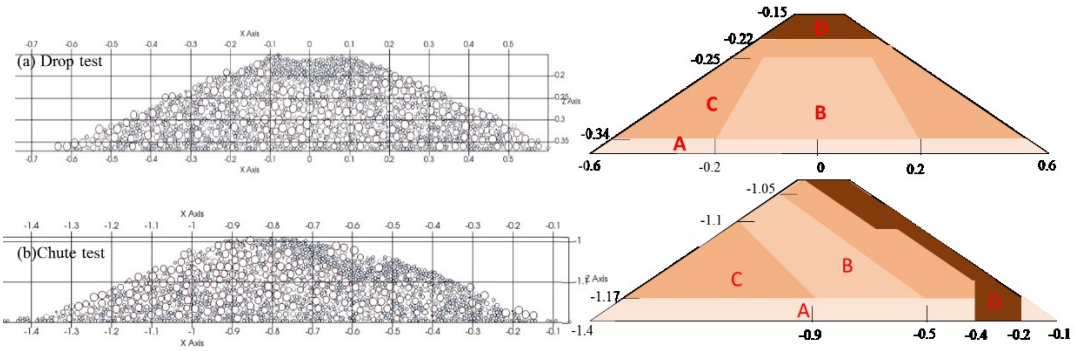

Fig. 9 The cross-slices (unit: m) through the center of the heap and the schematic representation of different porosity regions when the mass ratio is 3:2:5. Different color represents different porosity Zone.

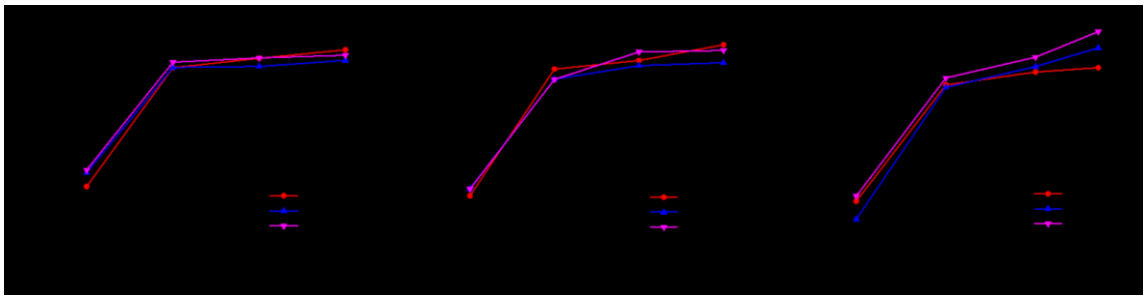

Fig. 10 The central porosity distribution along Z-axis of the pile with different original mass ratio and dump methods

Fig. 11 shows the relationship of the average porosity of different layers (along Z-axis) formed by two dump methods and different mass ratio of L/S (large particle/small particle), where layer 1, 2 and 3 expressed in **Fig. 3**. It can be seen that the difference of the average porosity between different layers along the vertical direction of the pile is obvious. The porosity decreases with the increase of L/S for all the two methods, which is consistent with the previous conclusion that the porosity increases with the increase of small particles. Comparing black (Drop Test) and pink (Chute Test) curves, different dump methods have some effect on the average porosity along the radial direction especially that in layer 1(at the beginning of dumps) with larger L/S. Because the Chute Test will aggravate the change of porosity along the radial direction compared with the Drop Test, which will cause the average porosity of the latter is larger than the former. Increasing the mass fraction of large particles will have more influence on the

Chute Test to cause uniformity of porosity distribution.

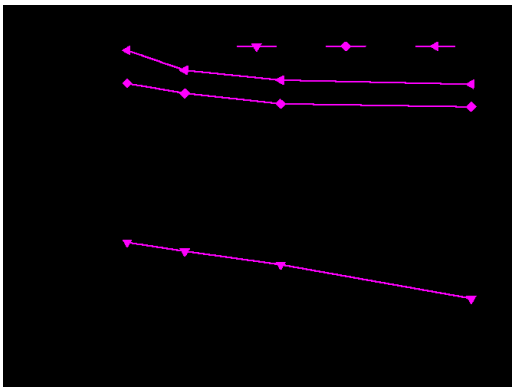

Fig. 11 The relationship of average porosity of different layers (along Z-axis) formed by two dump methods and the mass ratio (L/S) of large particles to small particles, Layer1,2 and 3 marked on Fig. 3.

4.2.2 Effects of external conditions on porosity distribution

Besides the effects of dump methods and particle mass fraction on spatial porosity distribution, some other operating conditions also influence the structure of porosity distribution of the sandpile. For example, the drop height (H, distance from the hopper exit to the table) in Drop Test and the properties of chute (length (L) and inclined angle (α), cf. **Fig. 1**) in Chute Test.

(1) Different drop heights of Drop Test

Fig. 12 shows the vertical cross-sections and cross-slices through the center of the heap with different drop heights (H=0.27, 0.37, 0.57, 0.8m). It can be seen that with the increase of the falling height, the region of small particles in the upper part of the pile (Zone D) becomes larger and Zone C becomes smaller. Because particles dropped from higher position will have larger kinetic energy when they reach to the heap surface, which indicates that it is easier for these particles to penetrate through the voids among large particles and reach to the lower layers. We also observe that a “pit”, which was smashed by fast moving particles, gradually appears in the upper part of the heap with the increase of the drop height.

Fig. 13 shows the porosity distribution along the Z-axis with different drop heights.

Because of the difference in the falling heights, we use different layers to represent different vertical positions of the heap instead of using specific values as before (**Fig. 10**). The porosity at the bottom (layer1 and layer 2) and the top (layer4) of the heap all has little change with different drop heights in the left figure of **Fig. 13**. However, the porosity in layer 3 has an evident difference, which increases with the increase of the drop height. Because small particles permeate into the region of large particles (Zone B), resulting in the increase of porosity in layer 3. The right figure in **Fig. 13** shows the average porosity of different layers along the Y-axis (F1, F2 … cf. **Fig. 3**), which reflects the radial variation of porosity and reveals that the porosity increases from the center to the edge (from black column to green column) of the heap. We can see that the drop height has the least effect on the layer 1 near the desktop as a result that the change of porosity in this region is mainly influenced by wall effect.

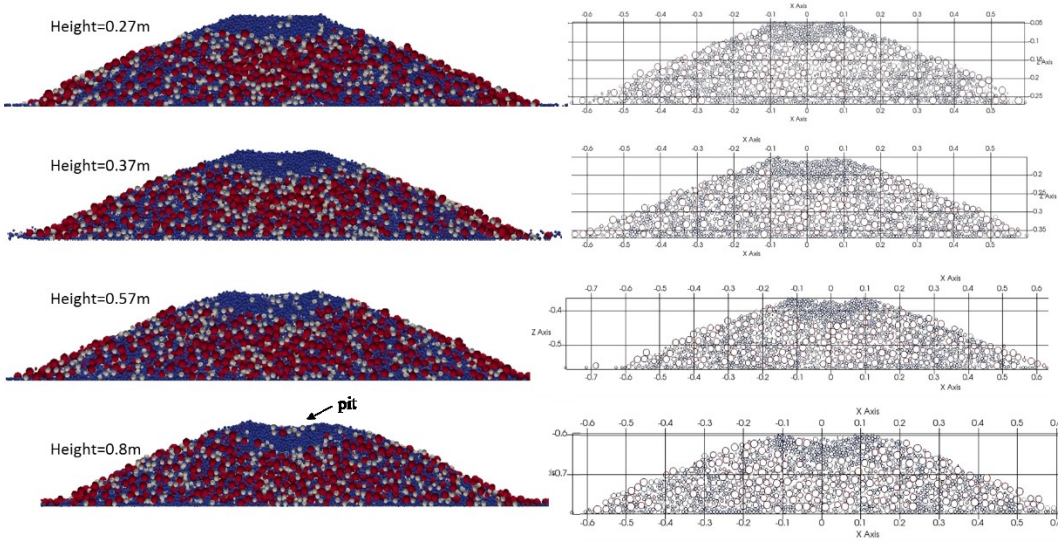

Fig. 12 Comparisons of the vertical cross-sections and cross-slices through the center of the heap (unit: m) with different drop height of Drop Method when the mass ratio of particles is 3:2:5.

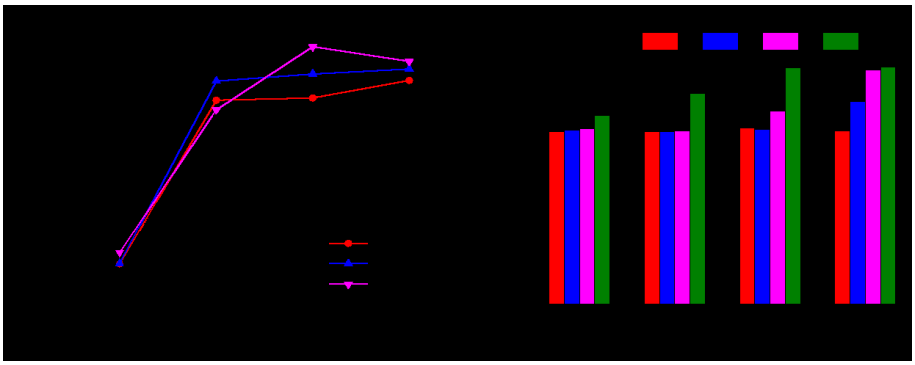

Fig. 13 The porosity distribution along the Z-axis and the average porosity of different layers of the piles with different drop heights in Drop Test

(2) Different chute properties of Chute Test

In the Chute Test, the properties of chutes are shown in **Table 5**. The length and inclined angle of the chute mainly influence the Zone C and Zone D of porosity. When the inclined angle of the chute is the same, the longer chute (chute 2) means that particles will lose more kinetic energy because of the friction force. Furthermore, after they leave the chute, they have the lower effective falling height to converting gravity potential energy into kinetic energy. In short, long chute and large inclined angle means small kinetic energy of falling particles.

Table 5 Properties of the chute used in Chute test

Chute	Length of chute(m)	Inclined angle of chute α (°)
Chute1	0.6	60
chute2	1.0	60
chute3	1.0	45

Fig. 14 shows the porosity distribution along layer 3 (cf. the red rectangles in **Fig. 15**) of the piles for different chutes. It is evident that the heap formed by chute 1 has the minimum porosity of the three and chute 3 has the maximum porosity. For the right half of the curve (range of X: -0.75—-0.55 m) in **Fig. 14**, the porosity increases from the center to the edge of the sandpile. For the left half, the regularity is quite weak. The reasons can be explained from the vertical cross-slices through the center of the heap with different chutes in **Fig. 15**. Comparing chute 3 with chute 1 and chute 2, the small particles flow down finally and form a “pure” small particle area of the heap formed by chute 3, which will lead to large porosity. Because when inclined angle of chute decreases (become steeper), the difference of velocity among the layered particles (large and small particles) on chute increases. Therefore, the large particles flow down faster on the surface and small particles flow down slower on the bottom. Comparing chute 1 and chute 2, small particles falling from chute 1 have higher kinetic energy to cause a dense structure because the chute 2 is longer than the chute 1.

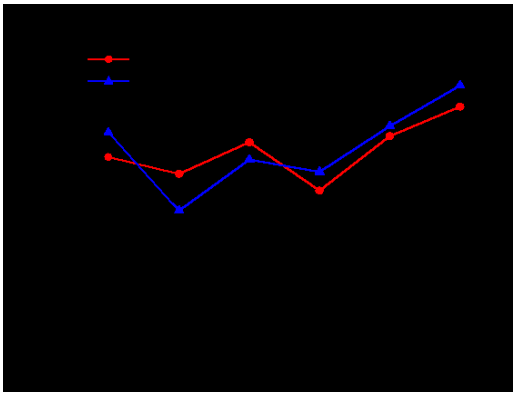

Fig. 14 The porosity distribution along layer 3 of the piles for different chutes in Chute Test

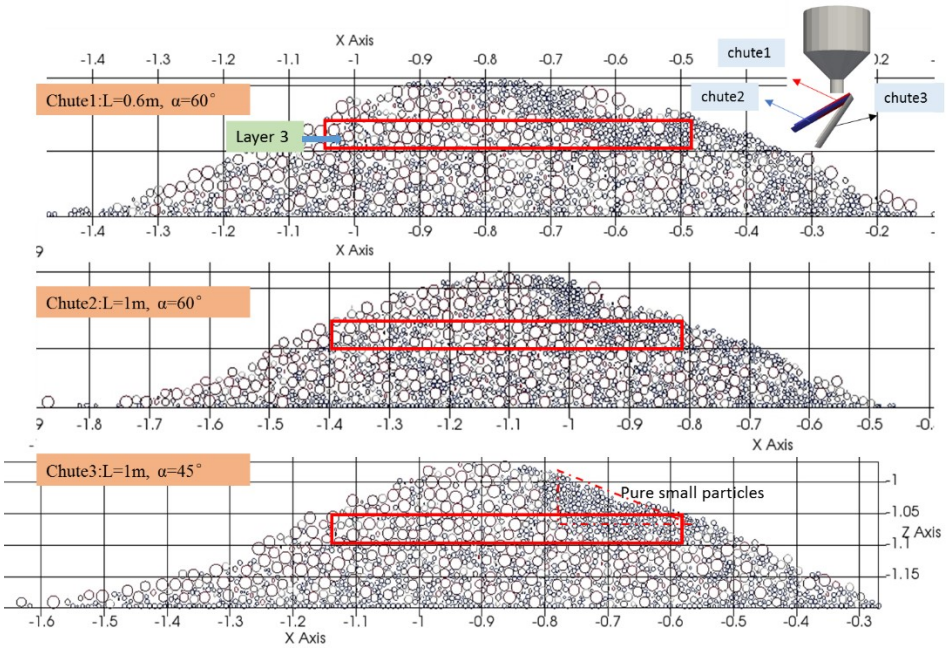

Fig. 15 Comparisons of the vertical cross-slices through the center of the heap (unit: m) with different chutes in **Table 5** of Chute Test when the mass ratio of particles is 3:2:5. The red rectangle is the center slice of layer 3

5. Conclusions

Porosity distribution of the sandpile formed by ternary size particles has been investigated by discrete element method. Before that, we have verified the physical parameters of pellet by comparing repose angles and bottom porosity distribution of the sandpile using experimental and numerical methods. The proper coefficient of rolling friction is 0.12 and coefficient of static friction is 0.15. The porosity distribution of

different layers of the sandpile has been studied; meanwhile, the effects of mass ratio of ternary size particles, dump method, drop height and properties of the chute on porosity distribution were also discussed in this work.

For the same layer of the pile, porosity increases with the decrease of the mass fraction of large particles or the increase of the fraction of small particles. Therefore, size segregation will lead to uneven porosity distribution. However, the relationship between radial porosity and mass fraction of medium particles is weak but the medium particles will influence the vertical porosity distribution. High porosity doesn't mean high segregation in sandpile, therefore, it's meaningful to study the change of porosity of the bed to control permeability and further control gas-solid reaction.

Different dump methods lead to different structures of porosity distribution of the pile. Nevertheless, we found that heaps formed by Drop Test and Chute Test both have four distinct porosity regions, Zone A, B, C and D, although the locations of the regions are not exactly the same. Zone A is a particle-mixing region dominated by small particles and Zone B is a large-particle region. Zone C is a particle-mixing region dominated by small and medium particles and Zone D is a small-particle region. In addition, the average porosity is Zone A<B<C<D. The extrusion of the upper particles to the bottom particles and the percolation of the small particles through the voids between large particles will have a significant impact on the porosity. In the Drop Test, increasing the drop height will decrease Zone D and increase Zone C, results in the increase of the porosity of the upper and the edges of the sandpile. In the Chute Test, decreasing the chute angle or the chute length will increase Zone D and decrease Zone C, results in the increase of the porosity of the upper of the sandpile.

Acknowledgments

We gratefully acknowledge financial support from The Program for Professor of Special Appointment (Eastern Scholar) at Shanghai Institutions of Higher Learning (No.TP2015039) and National Natural Science Foundation of China (No.51874171 and

51974182). The discrete element method simulations and analysis were conducted using LIGGGHTS 3.5.0 open source software.

Reference

[1] Li C, Honeyands T, O'Dea D, Moreno-Atanasio R. The angle of repose and size segregation of iron ore granules: DEM analysis and experimental investigation. Powder Technology 2017;320:257-72.

[2] Nikola T, Gallas JAC, Thorsten PS. Nonuniformities in the angle of repose and packing fraction of large heaps of particles. Physical Review Letters 2012;109:128001.

[3] Jullien R, Meakin P. A mechanism for particle size segregation in three dimensions. Nature 1990;344:425-7.

[4] Zhou Z, Zou R, Pinson D, Yu A. Angle of repose and stress distribution of sandpiles formed with ellipsoidal particles. Granular Matter 2014;16:695-709.

[5] Guises R, Xiang J, Latham J, Munjiza A. Granular packing: numerical simulation and the characterisation of the effect of particle shape. Granular Matter 2009;11:281-92.

[6] Höhner D, Wirtz S, Scherer V. A numerical study on the influence of particle shape on hopper discharge within the polyhedral and multi-sphere discrete element method. Powder Technology 2012;226:16-28.

[7] Coetzee C. Calibration of the discrete element method and the effect of particle shape. Powder Technology 2016;297:50-70.

[8] Zhao J, Li S, Jin W, Zhou X. Shape effects on the random-packing density of tetrahedral particles. Physical Review E Statistical Nonlinear & Soft Matter Physics 2012;86:03131-031306.

[9] Tangri H, Guo Y, Curtis JS. Packing of cylindrical particles: DEM simulations and experimental measurements. Powder Technology 2017;317:72-82.

[10] Guises R, Xiang J, Latham J-P, Munjiza A. Granular packing: numerical simulation and the characterisation of the effect of particle shape. Granular Matter 2009;11:281-92.

[11] Theuerkauf J, Witt P, Schwesig D. Analysis of particle porosity distribution in fixed beds using the discrete element method. Powder Technology 2006;165:92-9.

[12] Gan J, Yu A, Zhou Z. DEM simulation on the packing of fine ellipsoids. Chemical Engineering Science 2016;156:64-76.

[13] Wei H, Tang X, Ge Y, Li M, Saxén H, Yu Y. Numerical and experimental studies of the effect of iron ore particle shape on repose angle and porosity of a heap. powder technology 2019;353:12.

[14] STEPHENSON, J. L, STEWART, W. E. Optical measurements of porosity and fluid motion in packed beds. Chemical Engineering Science 1986;41:2161-70.

[15] Delmas H, Froment GF. A simulation model accounting for structural radial nonuniformities in fixed bed reactors. Chemical Engineering Science 1988;43:2281-7.

[16] Kondelik P, Horak J, Tesarova J. Heat and Mass Transfer in Heterogeneous Catalysis. Variation of Local Void Fraction in Randomly Packed Beds of Equilateral Cylinders. Industrial & Engineering Chemistry Process Design & Development 1968;7:29-51.

[17] Govindarao VMH, Froment GF. Voidage profiles in packed beds of spheres. Chemical Engineering Science 1986;41:533-9.

[18] Ridgway K, Tarbuck KJ. Voidage Fluctuations in Randomly- Packed Beds of Spheres Adjacent to a Containing Wall. Chemical Engineering Science 1968;23:1147-55.

[19] Rutgers R. Packing of Spheres1962.

[20] Yu AB, Standish N. Estimation of the porosity of particle mixtures by a linear-mixture packing model. Industrial & Engineering Chemistry Research 1991;30:1372-85.

[21] Yu AB, Zou RP. Modifying the Linear Packing Model for Predicting the Porosity of Nonspherical Particle Mixtures. Indengchemres 1996;35:3730-41.
[22] Behjani MA, Hassanpour A, Ghadiri M, Bayly A. Numerical Analysis of the Effect of Particle Shape and Adhesion on the Segregation of Powder Mixtures. Powders & Grains – International Conference on Micromechanics on Granular Media2017.
[23] Komatsu TS, Inagaki S, ., Nakagawa N, ., Nasuno S, . Creep motion in a granular pile exhibiting steady surface flow. Physrevlett 2001;86:1757.
[24] Alizadeh M, Hassanpour A, Pasha M, Ghadiri M, Bayly A. The effect of particle shape on predicted segregation in binary powder mixtures. Powder Technology 2017;319:313-22.
[25] Yu Y, Saxén H. Experimental and DEM study of segregation of ternary size particles in a blast furnace top bunker model. Chemical Engineering Science 2010;65:5237-50.
[26] Y.W. Yu, H. Saxén. Segregation behavior of particles in a top hopper of a blast furnace. Powder Technology 2014;262:233-41.
[27] Ketterhagen WR, Curtis JS, Wassgren CR, Kong A, Narayan PJ, Hancock BC. Granular segregation in discharging cylindrical hoppers: A discrete element and experimental study. Chemical Engineering Science 2007;62:6423-39.
[28] Wu S, Kou M, Xu J, Guo X, Du K, Shen W, et al. DEM simulation of particle size segregation behavior during charging into and discharging from a Paul-Wurth type hopper. Chemical Engineering Science 2013;99:314-23.
[29] Xu Y, Xu J, Liao Z, Pei Y, Gao L, Sun C, et al. DEM study on ternary-sized particle segregation during the sinter burden charging process. Powder Technology 2019;343:422-35.
[30] Guo Y, Wu CY, Thornton C. The effects of air and particle density difference on segregation of powder mixtures during die filling. Chemical Engineering Science 2011;66:661-73.
[31] Olaofe OO, Patil AV, Deen NG, van der Hoef MA, Kuipers JAM. Simulation of particle mixing and segregation in bidisperse gas fluidized beds. Chemical Engineering Science 2014;108:258-69.
[32] Peng Z, Joshi JB, Moghtaderi B, Khan MS, Evans GM, Doroodchi E. Segregation and dispersion of binary solids in liquid fluidised beds: A CFD-DEM study. Chemical Engineering Science 2016;152:65-83.
[33] Hameed S, Sharma A, Pareek V. Modelling of particle segregation in fluidized beds. Powder Technology 2019;353:202-18.
[34] Yang S, Sun Y, Zhang L, Chew JW. Segregation dynamics of a binary-size mixture in a three-dimensional rotating drum. Chemical Engineering Science 2017;172:652-66.
[35] Thomas N. Reverse and intermediate segregation of large beads in dry granular media. Physical Review E Statistical Physics Plasmas Fluids & Related Interdisciplinary Topics 2000;62:961-74.
[36] Rahman M, Shinohara K, Zhu HP, Yu AB, Zulli P. Size segregation mechanism of binary particle mixture in forming a conical pile. Chemical Engineering Science 2011;66:6089-98.
[37] Hong TW, Jung EJ, Lee DH. Segregation of glass beads in three-sectional tapered fluidized beds with ternary system. Powder Technology.
[38] Li C, Honeyands T, O'Dea D, Moreno-Atanasio R. DEM study on size segregation and voidage distribution in green bed formed on iron ore sinter strand. Powder Technology 2019;356:778-89.
[39] Ouchiyama N, Tanaka T. Porosity of a mass of solid particles having a range of sizes. Industrial & Engineering Chemistry Fundamentals 1981;20:66-71.
[40] Yu AB, Standish N. An analytical—parametric theory of the random packing of particles. Powder Technology 1988;55:171-86.

[41] Wei H, Tang X, Ge Y, Li M, Saxén H, Yu Y. Numerical and experimental studies of the effect of iron ore particle shape on repose angle and porosity of a heap. Powder Technology 2019;353:526-34.
[42] Mueller GE. Radial void fraction distributions in randomly packed fixed beds of uniformly sized spheres in cylindrical containers. Powder Technology 1992;72:269-75.
[43] Khalili A, Matyka M, Malek Mohammadi R, Weise J, Kuypers MMM. Porosity variation within a porous bed composed of multisized grains. Powder Technology 2018;338:830-5.
[44] Al Falahi F, Al-Dahhan M. Experimental investigation of the pebble bed structure by using gamma ray tomography. Nuclear Engineering and Design 2016;310:231-46.
[45] Götz J, Zick K, Heinen C, König T. Visualisation of flow processes in packed beds with NMR imaging: determination of the local porosity, velocity vector and local dispersion coefficients. Chemical Engineering and Processing: Process Intensification 2002;41:611-29.
[46] Zou RP, Gan ML, Yu AB. Prediction of the porosity of multi-component mixtures of cohesive and non-cohesive particles. Chemical Engineering Science 2011;66:4711-21.
[47] Mueller GE. A simple method for determining sphere packed bed radial porosity. Powder Technology 2012;229:90-6.
[48] Mueller GE. A modified packed bed radial porosity correlation. Powder Technology 2019;342:607-12.
[49] Hannsjörg F, Thomas Z, Florian H, Elias K, Gunther B. Numerical simulations of single phase reacting flows in randomly packed fixed-bed reactors and experimental validation. Chemical Engineering Science 2003;58:903-10.
[50] Tsotsas E, Schlünder EU. Heat transfer in packed beds with fluid flow: remarks on the meaning and the calculation of a heat transfer coefficient at the wall. Chemical Engineering Science 1990;45:819-37.
[51] Li CH, Finlayson BA. Heat transfer in packed beds—a reevaluation. Chemical Engineering Science 1977;32:1055-66.
[52] Cundall P, Strack O. A Discrete Numerical Mode For Granular Assemblies. Géotechnique 1979;29:47-65.
[53] Carrigy M. Experiments on the angles of repose of granular materials. Sedimentology 2010;14:147-58.
[54] Deboeuf S, Bertin E, Lajeunesse E, Dauchot O. Jamming transition of a granular pile below the angle of repose. The European Physical Journal B - Condensed Matter and Complex Systems 2003;36:105-13.
[55] Tsuji Y, Tanaka T, Ishida T. Lagrangian numerical simulation of plug flow of cohesionless particles in a horizontal pipe. Powder Technology 1992;71:239-50.
[56] Goniva C, Kloss C, Hager A, Pirker S. An open source CFD-DEM perspective. Proc Openfoam Workshop 2010.
[57] Kloss C, Goniva C, Hager A, Amberger S, Pirker S. Models, algorithms and validation for opensource DEM and CFD-DEM. Progress in Computational Fluid Dynamics An International Journal 2012;12:págs. 140-52.
[58] Standish N, Kilic A. Comparison of stop—start and continuous sampling methods of studying segregation of materials discharging from a hopper. Chemical Engineering Science 1985;40:2152-3.